Synaptopodin is necessary for *Shigella flexneri* intercellular spread.

Short title: Synaptopodin and bacterial infection

Authors: Jenna M. Vickery[1], Jody D. Toperzer[1], Julie E. Raab[1], Laurel L. Lenz[1], Sean P. Colgan[2], Brian C. Russo[1*]

1. Department of Immunology and Microbiology, University of Colorado School of Medicine, Aurora, CO 80045, USA
2. Division of Gastroenterology and Hepatology, Department of Medicine, University of Colorado School of Medicine, Aurora, CO 80045, USA

*Corresponding author
Email: brian.russo@cuanschutz.edu

Abstract

For many intracellular pathogens, their virulence depends on an ability to spread between cells of an epithelial layer. For intercellular spread to occur, these pathogens deform the plasma membrane into a protrusion structure that is engulfed by the neighboring cell. Although the polymerization of actin is essential for spread, how these pathogens manipulate the actin cytoskeleton in a manner that enables protrusion formation is still incompletely understood. Here, we identify the mammalian actin binding protein synaptopodin as required for efficient intercellular spread. Using a model cytosolic pathogen, *Shigella flexneri,* we show that synaptopodin contributes to organization of actin around bacteria and increases the length of the actin tail at the posterior pole of the bacteria. We show that synaptopodin presence enables protrusions to form and to resolve at a greater rate, indicating that greater stability of the actin tail enables the bacteria to push against the membrane with greater force. We demonstrate that synaptopodin recruitment around bacteria requires the bacterial protein IcsA, and we show that this recruitment is further enhanced in a type 3 secretion system dependent manner. These data establish synaptopodin as required for intracellular bacteria to reprogram the actin cytoskeleton in a manner that enables efficient protrusion formation and enhance our understanding of the cellular function of synaptopodin.

Keywords: Synaptopodin; *Shigella flexneri*; cell-to-cell spread; intercellular spread; intracellular pathogens; IcsA; Spa15; plasma membrane; protrusions; type 3 secretion system

Authors Summary

Intercellular spread is essential for many cytosolic dwelling pathogens during their infectious life cycle. Despite knowing the steps required for intercellular spread, relatively little is known about the host-pathogen interactions that enable these steps to occur. Here, we identify a requirement for the actin binding protein synaptopodin during intercellular spread by cytosolic bacteria. We show synaptopodin is necessary for the stability and recruitment of polymerized actin around bacteria. We also demonstrate synaptopodin is necessary to form plasma membrane structures known as protrusions that are necessary for the movement of these bacteria between cells. Thus, these findings implicate synaptopodin as an important actin-binding protein for the virulence of intracellular pathogens that require the actin cytoskeleton for their spread between cells.

51 **Introduction**

52 Many cytosolic-dwelling pathogens recruit actin-associated proteins to enable
53 intercellular spread between mammalian cells (1), including *Listeria* spp*., Rickettsia* spp*.,*
54 *Burkholderia* spp*., Mycobacterium marinum, Shigella* spp*.,* and poxviruses. The forces
55 generated from the polymerization of actin enable their intracellular motility and
56 movement between cells (2, 3). In order to polymerize actin, these organisms subvert
57 preexisting mammalian cytoskeletal pathways. Whereas the ability to repurpose the
58 cellular cytoskeleton is critical for their virulence, the molecular mechanisms that enable
59 actin motility among these pathogens are still incompletely understood (4-6).

60 Synaptopodin is the founding member of a family of natively unfolded proteins.
61 Approximately 20% of synaptopodin is composed of prolines, which prevent the assembly
62 of most secondary structures (7). Synaptopodin can function as a molecular scaffold that
63 interacts with multiple binding partners, including actin (8, 9). The mechanisms of
64 synaptopodin function remain poorly described. It is implicated in promoting actin fiber
65 formation through recruitment of Nck1 and through interaction with RhoA GTPase (10). It
66 promotes barrier integrity of the intestinal epithelium in response to butyrate by localizing
67 to tight junctions, where it interacts with actin fibers (11). In MDCK cells, synaptopodin
68 promotes cellular extrusion by forming a complex known as a contractomere, which
69 comprises synaptopodin, α-actinin-4, β-catenin, and myosin IIb and generates contractile
70 forces along the cell junction (12). Due to the critical role of actin-binding proteins during
71 infection by cytosolic pathogens, we sought to test whether and how synaptopodin
72 contributes to infection.

73 To examine the role of synaptopodin, we focused on interrogating its function during
74 infection by the model cytosolic pathogen *Shigella flexneri.* This Gram-negative bacterium
75 is a leading cause of bacillary dysentery, a form of bloody diarrhea (6). *S. flexneri* causes
76 disease by invading cells of the colonic epithelium and by spreading between cells in this
77 epithelial layer (13, 14). Cytosolic *S. flexneri* express IcsA at one bacterial pole (15). IcsA
78 binds Neural Wiskott-Aldrich syndrome protein (N-WASP), which then recruits the Actin
79 Related Protein 2/3 complex (Arp2/3) and promotes actin nucleation (16). The
80 polymerization of actin enables the bacteria to move in the cytosol of the cell (17). At the
81 periphery of the cell, some bacteria deform the plasma membrane into a protrusion
82 structure that pushes into the neighboring (recipient) cell (18), where it is actively
83 engulfed. In the recipient cell, these protrusions are resolved into double membrane
84 vacuoles. The bacteria quickly escape the double membrane vacuole into the cytosol,
85 where they can repeat this cycle of intercellular spread (19). Intercellular spread allows
86 the bacterium to access nutrients while evading the immune system, and both the
87 invasion of the colonic epithelium and the spread between cells are essential for
88 pathogenesis (5, 20-23). Defining the molecular mechanisms that promote the
89 intercellular spread of *Shigella* is essential to understand how this organism causes
90 disease.

91 Here, we identify the mammalian protein synaptopodin as required for *S.*
92 *flexneri* intercellular spread by enabling the formation of protrusions. Synaptopodin
93 promotes greater recruitment of actin around the bacteria in the cytosol and enables the
94 generation of tail structures with more optimized force vectors for generating protrusions.
95 Synaptopodin is recruited to bacteria in a manner that is dependent on the bacterial

96 protein IcsA, and its recruitment is additionally enhanced by a Spa15-dependent bacterial
97 protein. We show that synaptopodin function likely occurs in a manner distinct from
98 previously described pathways. Together, these data, using *S. flexneri* as a model,
99 identify synaptopodin as a critical cellular component that enables intercellular spread by
100 cytosolic pathogens.

101 **Results**

102 **Synaptopodin is required for efficient intercellular spread by *S. flexneri*.**

103 Since *S. flexneri* requires actin polymerization for intercellular spread (6) and since
104 synaptopodin is an actin-binding protein recently demonstrated to be essential for the
105 function of epithelial actin (11), we hypothesized that synaptopodin may contribute to *S.*
106 *flexneri* intercellular spread in intestinal epithelial cells. To test this, a plaque assay was
107 used to compare the efficiency of *S. flexneri* intercellular spread through a monolayer of
108 cells that produce synaptopodin to the efficiency of spread through monolayers that lack
109 synaptopodin. In this assay, the bacteria kill the cells as they spread, creating a zone of
110 clearance in the monolayer known as a "plaque". Whereas the number of plaques is a
111 function of the efficiency of bacterial invasion, the area of the plaques is a function of the
112 efficiency of intercellular spread. We measured the area of plaques formed in T84 human
113 colonic adenocarcinoma epithelial (T84) cells and Madin-Darby canine kidney (MDCK)
114 cells that either produced a control shRNA or a shRNA specific to synaptopodin (11, 12).
115 Synaptopodin protein levels are reduced by 80% in the T84 cells (11) and 85% in MDCK
116 cells (Fig. S1A-B). The plaques formed in monolayers of these cells were significantly
117 smaller when synaptopodin was knocked down compared to plaques formed in
118 monolayers of cells producing wild-type levels of synaptopodin (Fig. 1A-D).

119 We also compared the ability of *S. flexneri* to spread through monolayers of HeLa
120 cells, which are a model cell line to investigate *S. flexneri* infection. We used HeLa cells
121 producing a control shRNA or one of five synaptopodin-specific shRNAs. We observed
122 that plaques formed in monolayers of HeLa cells producing four of the five synaptopodin

123 specific shRNA were smaller than plaques formed in cells producing the control shRNA
124 (Fig. 1E-F and Fig. S1C-D). The four cell lines displaying reduced plaque size also
125 demonstrated a reduction in synaptopodin protein level as measured by western blot (Fig.
126 S1E-F). Thus, the smaller plaque size observed above was unlikely the result of non-
127 specific effects of an individual shRNA. *S. flexneri* replicated at a similar efficiency in T84,
128 MDCK, and HeLa cells that produced or lacked synaptopodin (Fig. S1G-L), indicating that
129 the reduction in plaque size is not due to differences in bacterial replication. Moreover,
130 since similar results were observed in T84, MDCK, and HeLa cells, these data indicate
131 that the requirement of synaptopodin for *S. flexneri* spread is unlikely to be specific for a
132 particular cell type.

133 We hypothesized that the spread defect observed with *S. flexneri* in synaptopodin
134 knockdown cells would be applicable to other pathogens that nucleate actin. *Listeria*
135 *monocytogenes* is a Gram positive bacterium that, like *Shigella,* requires actin-based
136 motility for intercellular spread (24). We compared the ability of *L. monocytogenes* to
137 spread through a monolayer of HeLa cells producing a control shRNA compared to cells
138 producing a shRNA specific to synaptopodin and used fluorescent microscopy to
139 measure the area of spread. Similar to the results observed with *S. flexneri, L.*
140 *monocytogenes* infection resulted in smaller areas of clearing in synaptopodin knockdown
141 cells compared to the control cells (Fig. S2), demonstrating that synaptopodin is required
142 for intercellular spread of *Listeria*. Together, these data show that *S. flexneri* and *L.*
143 *monocytogenes* require synaptopodin for efficient intercellular spread and that the
144 requirement of synaptopodin may be a general feature of intracellular bacterial pathogens
145 that spread.

146 **Synaptopodin is required for protrusion formation by *S. flexneri***

147 To investigate how synaptopodin contributes to efficient intercellular spread, we
148 focused on aspects of the bacterial intracellular life cycle that require actin. We assessed
149 the ability of bacteria to form plasma membrane protrusions in HeLa cells producing either
150 a control or a synaptopodin-specific shRNA. We determined the percentage of bacteria
151 present in a protrusion at 90 minutes of infection by examining the manner of actin
152 polymerized at the posterior pole of bacteria by immunofluorescence microscopy. A
153 smaller percentage of bacteria in synaptopodin knockdown cells were present in plasma
154 membrane protrusions compared the percentage of bacteria in protrusions in control cells
155 (Fig. 2A-B), demonstrating that synaptopodin is required for efficient protrusion formation.

156 Synaptopodin is associated with the bundling and elongation of actin filaments in
157 cells (25, 26), but actin intensity at the plasma membrane near protrusions was similar in
158 the presence and absence of synaptopodin (Fig. 2C), indicating that the protrusion defect
159 is not due to defects in the amount of actin recruited to protrusions. Protrusion formation
160 is also dependent on actin that is polymerized by formins. The formin mDia1 is required
161 for formation of protrusions by *S. flexneri* and *L. monocytogenes* (27, 28). mDia1 was
162 efficiently recruited to protrusions formed in control or synaptopodin knockdown cells (Fig.
163 S3), indicating reduced mDia1 levels around bacteria are not driving the reduction in
164 protrusion formation in the relative absence of synaptopodin. The length of the protrusion
165 is more generally associated with the efficiency of intercellular spread (29). Protrusion
166 lengths were similar irrespective of synaptopodin levels in HeLa cells (Fig. 2D), indicating
167 that the requirement for synaptopodin was not associated with protrusion length.

168 We next investigated the kinetics of protrusion formation by *S. flexneri* to further
169 clarify the role of synaptopodin in the development of membrane protrusions. To visualize
170 the formation of protrusions, intracellular bacteria were tracked by time-lapsed
171 microscopy during infection of HeLa cells that produce a YFP that is anchored to the
172 plasma membrane (30). Bacteria in control cells formed protrusions at a greater velocity
173 than bacteria in cells lacking synaptopodin (Fig. 2E-F). Protrusions formed in the
174 presence of synaptopodin were also faster to resolve, lasting an average of 18 min in
175 control cells compared to 27 min in synaptopodin deficient cells (Fig. 2G). These data
176 show synaptopodin enables more rapid formation and resolution of protrusions.

177 **Synaptopodin regulates actin tail formation by *S. flexneri***

178 The ability to efficiently assemble an actin tail in the cell cytosol is associated with
179 efficient protrusion formation at the plasma membrane (31). We hypothesized that the
180 defects in protrusion formation were the result of aberrant actin tail formation. To test this,
181 we infected HeLa cells with *S. flexneri* and characterized the actin tails. Although a similar
182 percentage of bacteria formed actin tails in the control and synaptopodin knockdown cells
183 (Fig. 3A-B), actin tails that formed in the synaptopodin knockdown cells were significantly
184 shorter than actin tails in the control cells (Fig. 3C). In MDCK cells, the actin tails formed
185 by *S. flexneri* in the control cells were also significantly longer than tails in the
186 synaptopodin knockdown cells (Fig. S4A-B). Previous studies have shown that the length
187 of the actin tails correlates with the rate of actin polymerization and the speed bacteria
188 move in the cytosol (32). Since we observed shorter tails in HeLa and MDCK cells, it
189 suggested to us that the rate of actin polymerization could be reduced in the absence of
190 synaptopodin and would result in *S. flexneri* moving more slowly through the cytosol of

191 the cells. To test this, time-lapsed microscopy was performed on intracellular bacteria in
192 HeLa cells to evaluate the efficiency of actin-based motility. In contrast to our expectation
193 based on the length of the actin tails, the bacterial velocity was similar in the control and
194 synaptopodin knockdown cells (Fig. 3D-E).

195 In addition to differing in length, the width of the actin tails at the base of the
196 bacteria was wider in control HeLa cells than in synaptopodin knockdown HeLa cells (Fig.
197 S5A-B). Interestingly, actin tails at the base of the bacteria in MDCK cells not significantly
198 different in width between control and synaptopodin knockdown cells (Fig. S4C). We also
199 noted additional phenotypic changes to the tails in HeLa cells lacking synaptopodin.
200 Polymerized actin was more frequently present along the lateral sides of the posterior
201 end of bacteria in the control cells compared to in synaptopodin knockdown cells (Fig.
202 S5C). During bacterial infection or when examining actin polymerization around lipid
203 vesicles, the actin on the sides of the bacteria or vesicle creates an inward force at the
204 base that is predicted to contribute to the propulsive force (33, 34). Seeing that there was
205 no difference in the velocity at which *S. flexneri* traveled whether or not actin extended
206 along the sides of the bacteria, we hypothesized that the additional actin may stabilize
207 the tail and keep the actin tail in line with the bacteria, which we anticipated would stabilize
208 the path along which the bacteria travels. To investigate this, we measured the angle at
209 which the actin tail extended from the posterior pole of the bacteria. We set actin tails that
210 formed completely in line with the longitudinal axis of the bacteria at 0° and deviations
211 from this alignment resulted in an increased angle. In the synaptopodin knockdown cells,
212 the actin tails were less aligned with the bacteria's longitudinal axis than the tails
213 associated with bacteria in the control cells, which resulted in a greater angle from the

214 longitudinal axis for bacteria in synaptopodin knockdown cells (Fig. S5D). These data
215 show that synaptopodin enables actin presence along the lateral sides near the posterior
216 end of the bacteria and that synaptopodin enables the actin tail to be more in line with the
217 bacteria. We theorized that the angle of the actin tail would decrease the forward
218 momentum that the actin nucleation creates at the base of the bacteria. We used the
219 formula $[sin\ (angle\ of\ the\ tail(\theta))\ +\ cos(angle\ of\ the\ tail(\theta))]$ to calculate the force of
220 the actin tail on the bacteria. We then calculated the percentage of force that contributed
221 to the forward momentum of the bacteria by the formula $[cos\ (angle\ of\ the\ tail(\theta))\ /$
222 $total\ force]\ *\ 100$. The percentage of the theoretical forward movement of bacteria in
223 the control cells is higher than in the synaptopodin knockdown cell lines (Fig. S5E). We
224 hypothesized that the defects in the actin tail length, width, organization, and angle of
225 attachment would lead to a defect in the linear trajectory of the bacteria in the absence of
226 synaptopodin. We tracked intracellular bacteria with time-lapsed microscopy to evaluate
227 the linear trajectory. We calculated the distance an individual bacteria traveled and
228 divided it by the distance of the theoretical most efficient path – a straight line. A bacterium
229 that took the most efficient path would have a linear trajectory ratio of 1.0. We observed
230 that bacteria deviated further from an ideal path in cells lacking synaptopodin compared
231 to control cells (Fig. S5F), which showed that bacteria traveled along a straighter path in
232 the presence of synaptopodin.

233 Since we show that *L. monocytogenes* also requires synaptopodin to efficiently
234 spread between cells, we also tested whether the length of actin tails was similarly
235 decreased during *L. monocytogenes* infection of HeLa cells. Similar to *S. flexneri,* actin

236 tails formed by *L. monocytogenes* were longer in the presence of synaptopodin compared
237 to the actin tails formed in the absence of synaptopodin (Fig. S6).

238 Altogether, these data show that synaptopodin regulates the length of actin tails
239 during bacterial intercellular spread (Fig. 3F) and that in HeLa cells there are additional
240 defects in actin tails formed by *S. flexneri* in the absence of synaptopodin (Fig. S5G).
241 Interestingly, these shorter tails did not cause a defect in the velocity of actin-based
242 motility for *S. flexneri* in the cytosol.

243 **Synaptopodin colocalizes with actin around *S. flexneri***

244 Based on the requirement for synaptopodin in organizing the actin tail and in
245 forming protrusions, we hypothesized that *S. flexneri* would recruit synaptopodin during
246 intracellular infection. To test this, we infected HeLa and MDCK cells with *S. flexneri* and
247 used immunofluorescence microscopy to visualize synaptopodin localization in cells.
248 Both cell lines showed that synaptopodin was recruited to bacteria in the cytosol (Fig. S7-
249 8). Furthermore, synaptopodin localizes to bacteria that also displayed actin recruitment,
250 but synaptopodin was not observed around bacteria that failed to recruit actin (Fig. S7-
251 8). These data show that synaptopodin is recruited to bacteria that nucleate actin
252 polymerization.

253 Knockdown of synaptopodin caused fewer bacteria to recruit synaptopodin (Fig.
254 S7A-B), and among the bacteria that showed synaptopodin recruitment, there was a
255 reduction in the intensity of synaptopodin (Fig. S7C). Although loss of synaptopodin did
256 not reduce the percentage of bacteria that formed an actin tail (Fig. 3B), the knockdown
257 of synaptopodin significantly reduced the number of bacteria that recruited actin (Fig.

258 S7D), yet there was not a significant difference in the intensity of the actin signal among
259 the bacteria that recruited actin in the presence or absence of synaptopodin in these
260 experiments (Fig. S7E). These data show that synaptopodin is recruited to intracellular
261 bacteria and promotes actin polymerization around bacteria.

262 **Synaptopodin promotes myosin IIb recruitment around *S. flexneri*.**

263 The localization of IcsA to the posterior pole of *S. flexneri* results in the recruitment
264 of N-WASP and the Arp2/3 complex and enables the initiation of actin polymerization and
265 bacterial motility (16). Synaptopodin is known to regulate this process through another
266 protein Nck1 (35). Synaptopodin promotes Nck1 abundance in cells by blocking c-Cbl-
267 mediated ubiquitination of Nck1, and Nck1 assists in N-WASP and Arp2/3 recruitment
268 during vaccina virus infection (35, 36). We tested whether the defect in actin recruitment
269 in cells lacking synaptopodin was due to a disruption in this synaptopodin-Nck1-Arp2
270 pathway. We observed a similar percentage of bacteria that recruited Arp2, and these
271 bacteria were associated with similar levels of Arp2 as measured by the intensity of the
272 fluorescent signal of Arp2 around bacteria (Fig. S9A-C). We tested whether Nck1 was
273 recruited to the bacteria during intracellular infection. We found no evidence of Nck1
274 recruitment in our cells (Fig. S9D). We examined the ability of *S. flexneri* to recruit N-
275 WASP and observed a similar percentage of bacteria recruited N-WASP (Fig. S9E-F).
276 Among the bacteria that recruited N-WASP, the amount of N-WASP was similar
277 irrespective of synaptopodin levels (Fig. S9G). Together, these data show that
278 synaptopodin facilitates actin organization around the bacteria, but it remains uncertain
279 how synaptopodin alters the organization of actin in our system.

280 We further sought to examine whether we could identify interactions that were
281 important for the formation of the protrusion. Synaptopodin is described to interact with
282 non-muscle myosin IIb (myosin IIb) and α-actinin-4 at the plasma membrane, where
283 together they form the contractomere complex that generates force so as to enable the
284 extrusion of cells from a monolayer (12). Recent work shows that α-actinin-4 is present
285 at actin structures formed during *S. flexneri* infection (1). We tested for the recruitment of
286 myosin IIb and α-actinin-4 by immunofluorescence microscopy. Interestingly, a smaller
287 percentage of bacteria recruited myosin IIb in the absence of synaptopodin (Fig. 4A and
288 B), but among the bacteria that recruited myosin IIb, there was a similar abundance of
289 myosin IIb as measured by fluorescent intensity irrespective of synaptopodin levels (Fig.
290 4C). We observed similar levels of α-actinin-4 recruited to bacteria and similar abundance
291 of α-actinin-4 around the bacteria as measured by fluorescent intensity in control and
292 synaptopodin knockdown cells (Fig. 4D-F). Altogether, these data indicate that
293 synaptopodin presence enhances myosin IIb recruitment around *S. flexneri*.

294 **IcsA and the type 3 secretion system regulate synaptopodin recruitment around *S.***
295 ***flexneri.***

296 *S. flexneri* requires a type three secretion system (T3SS) for intercellular spread (37-39).
297 This type 3 secretion system delivers over 30 bacterial virulence proteins (effectors) into
298 the cell (40). The delivered effectors coopt cellular signaling pathways and enable *S.*
299 *flexneri* to thrive in the intracellular environment. Here, we sought to determine whether
300 synaptopodin was recruited around the bacteria indirectly due to the high concentrations
301 of polymerized actin around the bacteria, as a result of direct recruitment by *S.*

302 *flexneri* secreted proteins, or both. To do so, we tested whether IcsA or the type 3
303 secreted effector proteins contributed to synaptopodin recruitment by investigating
304 synaptopodin localization during cellular infection by several bacterial mutants: *S. flexneri*
305 △*icsA* is unable to polymerize actin; *S. flexneri* △*spa15* lacks a chaperone for nine type 3
306 secreted effector proteins – the absence of Spa15 results in these proteins being unstable
307 and degraded (41); *S. flexneri* △*mxiE* lacks the MxiE transcription factor that is necessary
308 to transcriptionally activate the expression of more than 25 effectors – in the absence of
309 MxiE these effectors are not produced in the bacteria (42-44). Together, the absence of
310 Spa15 and MxiE enabled us to examine whether more than 30 effectors contribute to
311 synaptopodin recruitment as two pooled groups. We infected HeLa cells with these
312 mutants and quantified the percentage of bacteria that showed recruitment of
313 synaptopodin and/or actin, and we measured the intensities of these recruited proteins.
314 As expected, *S. flexneri* △*icsA* did not recruit actin or form actin tails during intracellular
315 infection (Fig. 5A-B). Interestingly, bacteria lacking IcsA also did not recruit synaptopodin
316 (Fig. 5C). A similar percentage of wild-type bacteria and bacteria lacking MxiE recruited
317 actin and synaptopodin (Fig. 5A-C). Loss of Spa15 resulted in a smaller percentage of
318 bacteria that recruited actin compared to wild-type bacteria, but a similar percentage of
319 wild-type and Spa15 deficient bacteria recruited synaptopodin (Fig. 5C). When we
320 examined the amount of actin and synaptopodin recruited around bacteria by comparing
321 the intensity of fluorescent signal, we observed that except for the *icsA* mutant, actin was
322 efficiently recruited around bacteria (Fig. 5D). Yet when we examined the amount of
323 synaptopodin around bacteria, we observed that bacteria lacking Spa15 or IcsA, but not
324 MxiE, recruited less synaptopodin than wildtype bacteria (Fig. 5E). Altogether these data

325 show that bacterial recruitment of synaptopodin is dependent on *S. flexneri* protein IcsA

326 and one or more type 3 secretion system effector proteins regulated by Spa15.

327 **Discussion**

328 Many cytosolic-dwelling pathogens require the subversion of actin and host
329 proteins for intracellular motility. These pathogens remodel the cytoskeleton and plasma
330 membrane resulting in the formation of protrusions, which facilitate intercellular spread.
331 Here, we show that the mammalian protein synaptopodin is recruited to *S. flexneri* in a
332 manner that is dependent on the bacterial protein IcsA and the type 3 secretion system.
333 We show that synaptopodin enables efficient *S. flexneri* intercellular spread by increasing
334 the velocity at which the plasma membrane protrusions form and resolve.

335 Previous studies have shown that the length of the actin tail formed by *Listeria*
336 *monocytogenes* directly correlates with the rate of actin polymerization and the
337 intracellular velocity of the bacteria (32). Although synaptopodin presence enabled longer
338 actin tails to form (Fig. 3C, S4, and S6), synaptopodin loss did not alter the speed the
339 bacteria moved in the cytosol (Fig. 3D-E). Moreover, proteins associated with actin
340 nucleation, such as N-WASP and Arp2, were efficiently recruited to bacteria irrespective
341 of synaptopodin (Fig. S9A-C and E-G). These findings suggest that rather than altering
342 the rate of actin polymerization, synaptopodin may stabilize the actin filaments that are
343 already formed leading to the generation of longer actin tails. Similar to our findings, the
344 stabilization of F-actin by synaptopodin enables the formation of dendritic spines in
345 neurons (26, 45). Although the tail length did not correlate with bacterial speed in the
346 cytosol, protrusions formed more slowly in the absence of synaptopodin (Fig. 2F). We
347 speculate that this could occur because the rate of addition of new actin monomers as
348 well as the rate of loss of old actin monomers may both contribute to the speed at which
349 the protrusions form.

350 Along with shorter actin tails, bacterial tails formed in the synaptopodin knockdown
351 HeLa cells were less aligned with the longitudinal axis of the bacteria and lacked actin
352 recruitment along the sides of the bacteria. Here, our data indicate that the additional
353 actin provides a stabilizing effect by maintaining actin polymerization in line with the
354 bacterial longitudinal axis and enabling the bacteria to move in a more directed manner
355 forward (Fig. S5F). In MDCK cells, synaptopodin was associated with decreased length
356 of actin tails, but not the width (Fig. S4). Our data indicate that a reduction of actin on the
357 sides of the bacteria does not affect the velocity of cytosolic bacteria (Fig. 3). Rather, we
358 speculate that this specific synaptopodin-dependent localization of actin in HeLa cells
359 may be necessary at the membrane where the bacteria experience additional forces
360 during the formation of the protrusion.

361 Previous studies have shown that synaptopodin forms a force-generating complex
362 with α-actinin-4 and myosin IIb that pulls from the pointed-end toward the barbed-end of
363 the actin filaments. This force generation results in the buckling of actin filaments and
364 pulls on the plasma membrane in a manner that causes cells to extrude from a monolayer
365 (12). One role for synaptopodin could be to function as a force-generating complex that
366 pushes actin filaments into the protrusion structure and enables protrusion formation to
367 be more efficient, but we anticipate this is unlikely to occur during infection. The barbed
368 end of the filaments would be proximal to the bacteria where the incorporation of new
369 actin monomers occurs. Thus, force generation by synaptopodin as described for the
370 contractomere complex would generate a resistive force against protrusion formation by
371 pulling the barbed end of actin back into the cell rather than pushing them out of the cell.
372 Yet, we observe protrusions form faster with synaptopodin (Fig. 2E-G). An intriguing

373 possibility is that synaptopodin, as part of the contractomere complex, is anchored at the
374 plasma membrane and pulls the membrane along the actin filaments toward the bacteria.
375 By pulling membrane into the protrusion, the contractomere complex would both create
376 some slack in the membrane so as to enable the bacteria to more efficiently form the
377 protrusion structure and would provide some mechanism for how the significant amount
378 of plasma membrane is redirected into the protrusion. Although we have not seen
379 descriptions of myosin IIb during *S. flexneri* infection, previous reports do indicate roles
380 for myosin IIa and myosin X (29, 46), and hypothesize that these myosins could function
381 in a similar manner by pulling the plasma membrane into the protrusion (29). A second
382 possibility is that the presence of synaptopodin simply stabilizes the actin fibers, as
383 described above, so that the loss of actin monomers is less efficient and the fibers remain
384 longer in the protrusion for a greater period of time, thereby promoting the formation of
385 the protrusion structure.

386 *Shigella* spp., *Listeria* spp., *Rickettsia* spp., *Burkholderia* spp., *Mycobacterium*
387 *marinum,* and pox viruses such as vaccina virus are all examples of pathogens that
388 require actin nucleation for their virulence. Recent studies show that mitochondria use
389 similar mechanisms of motility by generating actin comet tails so as to enable organelle
390 segregation during mitosis (47). Our findings show that synaptopodin is a critical regulator
391 of actin polymerization and organization during *S. flexneri* intercellular spread, and we
392 anticipate that our findings represent a more general role of synaptopodin-dependent
393 regulation of actin dynamics in cells and during infection.

394 **METHODS**:

395 **Bacterial Culture:**
396
397 *S. flexneri* strain 2457T is used in this study, and all mutants are derived from this strain
398 (14). *S. flexneri* strains were cultured in trypticase soy broth (TCS) at 37°C and shaken
399 at 250 rpm. Bacteria were transformed with pROEX-Aqua [Addgene; plasmid #42889,
400 (48)] or pBR322-mCherry for live and fixed microscopy. *L. monocytogenes* strain 10403S
401 is used in this study (49). *L. monocytogenes* strains were cultured in trypticase soy broth
402 (TCS) at 37°C.

403 **Cell Culture:**

404 HeLa cells, MDCK cells (gift of Vivian Tang), and T84 cells were maintained at 37°C in
405 5% CO_2. HeLa and MDCK cells were grown in Dulbecco's modified Eagle's Medium
406 (DMEM) supplemented with 10% fetal bovine serum (FBS). T84 cells were grown in
407 Advance DMEM supplemented with 10% FBS and 1% L-glutamine. The generation of
408 T84 cells producing control or synaptopodin specific shRNA were previously described
409 (11), and the generation of MDCK cells producing control or synaptopodin specific shRNA
410 were previously described (12). HeLa cells producing shRNA targeting synaptopodin
411 were generated using retroviral transduction followed by selection with 5 μg/mL
412 puromycin.

413 **Virus Preparation:**

414 3 million 293T cells were seeded in 100 mm dishes in DMEM supplemented with 10%
415 FBS for 24 hours prior to transduction. Cells were transduced with psPAX2 (Addgene,

416 12260), pVSVg, and either pLKO.5 (SHC216) for control shRNA or a synaptopodin
417 specific shRNA (TRCN0000218429, TRCN0000230911, TRCN0000230913,
418 TRCN0000230912, TRCN0000218782), or pmbYFP (Gift of Hervé Agaisse). Plasmids
419 were transfected into cells using calcium phosphate, which was added dropwise to 293
420 cells, which were then left to incubate at 37°C for 24 hours. The next day, the cells were
421 washed twice, and the media was replaced with fresh DMEM supplemented with 10%
422 FBS. After incubation for an additional 24 hours, the culture supernatant containing the
423 viral particles was collected, passed through a 0.45 µm filter, and stored at -20°C.

424 **Viral Transduction:**

425 3 x 10^5 HeLa cells were seeded in 6-well plates and 2 mL of filtered 293 supernatant
426 containing 4mM polybrene was added to the cells and centrifuged for 2 hours at 1000 *g*
427 at 30°C. Cells then were incubated at 37°C for 48 hours, and the media was replaced
428 with DMEM supplemented 10% FBS and 5 µg/mL puromycin. Resistant cells were
429 expanded. For cells transduced with virus encoding the membrane anchored YFP, cells
430 were sorted at the Flow Cytometry Shared Resource Laboratory in the Department of
431 Immunology and Microbiology to enrich for YFP positive cells.

432 **Plaque Assay:**

433 Cells were seeded at 8 x 10^5 cells per well in 6-well plates. The next day, cells were
434 infected with *S. flexneri* at a multiplicity of infection (MOI) of 0.2 for HeLa cells or a MOI
435 of 20 for MDCK cells and T84 cells. Bacteria were centrifuged onto cells at 800 *g* for 10
436 minutes and incubated at 37°C in 5% CO_2 for 90 min. Media was replaced with DMEM
437 containing 10% FBS, 25 µg/mL gentamicin, and 0.5% agarose, and the cells were

438 incubated for 48 hours. To visualize plaques, a second overlay was added with 0.7%
439 agarose in DMEM with 10% FBS, 25 µg/mL gentamicin, 0.1% neutral red. Following
440 incubation for at least 4 hours, the plates were imaged with an ImmunoSpot S6 Universal
441 Visible/Fluorescent Analyzer (Cellular Technology Limited). Analysis of the plaque area
442 was performed using a pipeline generated in ImageJ in which images were thresholded
443 to remove background, pixel intensity was converted to a binary, and the images were
444 segmented into objects; objects matching plaques on unmodified images were selected,
445 and their area was quantified, as done previously (38).

446 **Spread Assay by Microscopy:**

447 Cells were seeded at 7 x 10^5 cells per well in 6-well plates onto sterile coverslips. The
448 next day, cells were infected with *Listeria monocytogenes* at a MOI of 15 in PBS. The
449 bacteria were centrifuged onto cells at room temperature at 800 *g* for 10 minutes. The co-
450 culture was incubated at 37°C with 5% CO_2 for 45 mins. Excess bacteria were removed
451 by three successive washes with HBSS. Any remaining extracellular bacteria were killed
452 by incubation in DMEM supplemented with 10% FBS and 25 µg/mL gentamicin. The
453 infection was incubated for an additional 24 or 48 hours and then were fixed with 3.7%
454 paraformaldehyde for at least 20 minutes at room temperature. The cells were
455 permeabilized with 1% triton X-100 in PBS for 30 minutes at room temperature. The cells
456 were washed 5 times with PBS. Cells were stained with phalloidin conjugated to Alexa
457 Flour 750 (Invitrogen A30105) washed with PBS, stained with Hoechst 33342 (Biotech
458 No. 5117), washed twice with PBS, and mounted with Prolong Diamond Antifade
459 Mountant (ThermoFisher, P36930). Images were taken at random at 20x magnification.

460 5 fields of view of infection were analyzed per condition per experiment and area of spread
461 was measured with NIS elements.

462 **Quantification of Intracellular Bacteria:**

463 T84 cells were seeded at 8 X 10^5 cells per well, and HeLa cells and MDCK cells were
464 seeded at 4 X 10^5 cells per well in a 6-well plate. The next day, cells were infected with
465 *S. flexneri* at an MOI of 200. The bacteria were centrifuged onto cells at room temperature
466 at 800 *g* for 10 minutes. The co-culture was incubated at 37°C with 5% CO_2 for 45
467 minutes. Excess bacteria were removed by three successive washes with HBSS. Any
468 remaining extracellular bacteria were killed by incubation in DMEM supplemented with
469 10% FBS and 25 µg/mL gentamicin. The infection was incubated for an additional 1, 2,
470 or 3 hours. The cells were washed three times with HBSS, and then the cells were lysed
471 with 0.02% SDS in HBSS. The cell lysates with intact bacteria were serially diluted in TCS
472 broth and plated onto TCS agar to determine the intracellular CFU.

473 **Western Blots:**

474 SDS-PAGE gels were transferred to nitrocellulose using a Turbo semi dry transfer
475 apparatus (BioRad). For detection of antigen, 1:100 rabbit anti-synaptopodin (Abcam,
476 ab224491) was incubated overnight at 4°C in 5% milk. The next day, blots were incubated
477 with 1:5,000 goat anti-rabbit (Jackson Immuno Research Labs, 111-035-144) for 2 hours
478 at room temperature or 1:10,000 anti-β-actin conjugated to HRP (Sigma A3854) for 1 hour
479 at room temperature. Western blots were developed, and the signal was acquired by a
480 G:Box (Syngene). Band intensity was measured using ImageJ (NIH) with the background
481 subtracted.

482 **Localization of Host Proteins:**

483 HeLa cells or MDCK cells were seeded at 8 X 10^5 cells per well in a 6-well plate and
484 cultured for 24 hours (HeLa) or 48 hours (MDCK). On the day of the infection, media was
485 replaced with DMEM with 10% FBS and 100 mM IPTG. Cells were infected with
486 designated strains of *S. flexneri* harboring pROEX-Aqua. Bacteria were centrifuged onto
487 cells at 800 *g* for 10 minutes and incubated at 37°C in 5% CO_2. At 45 minutes of infection,
488 cells were washed three times with HBSS, and media was replaced with DMEM with 10%
489 FBS, 25 µg/mL gentamicin, and 100 mM IPTG. After an additional 45 minutes, cells were
490 fixed with 3.7% paraformaldehyde for at least 20 minutes at room temperature. The cells
491 were permeabilized with 1% triton X-100 in PBS for 30 minutes at room temperature. The
492 cells were washed 5 times with PBS and incubated in PBS with 10% FBS and 1:100 rabbit
493 anti-synaptopodin (Abcam, ab224491), 1:1000 rabbit anti-N-WASP (Santa Cruz
494 Biotechnology Inc, sc100964), 1:500 rabbit anti-α-actinin-4 (Abcam, ab108198), 1:50
495 rabbit anti-mDia1 (Abcam, AB129167), 1:500 mouse anti-myosin IIb (Santa Cruz
496 Biotechnology Inc, sc-376942), or 1:50 goat anti-Arp 2 (Novus Biologicals, NB100-1037)
497 overnight at 4°C. The cells were washed with PBS, incubated with 1:100 donkey anti-
498 rabbit conjugated with Alexa Fluor 594 (ThermoFisher, A-21207), goat anti-rabbit
499 conjugated with Alexa Fluor 750 (ThermoFisher, A21039), donkey anti-mouse conjugated
500 with Alexa Fluor 594 (Invitrogen, A32744), or donkey anti-goat conjugated with Alexa
501 Fluor 594 (ThermoFisher, A32758) for 2 hours at room temperature, and washed with
502 PBS. Cells were stained with phalloidin conjugated to Alexa Flour 750 (Invitrogen
503 A30105) or Alexa Fluor 647 (Invitrogen, A22287), washed with PBS, stained with Hoechst

504 33342 (Biotech No. 5117), washed twice with PBS, and mounted with Prolong Diamond
505 Antifade Mountant (ThermoFisher, P36930).

506 **Live Imaging for Speed of Cytosolic Bacteria and of Protrusion Formation:**

507 HeLa cells expressing a membrane-anchored yellow fluorescent protein were seeded at
508 8 X 10^5 cells per well on Ibid 2-well chamber slides (Ibidi, 80286). The next day, media
509 was replaced with DMEM supplemented with 10% FBS and 100 mM IPTG, cells were
510 infected with designated strains of *S. flexneri* harboring the pROEX-Aqua plasmid at an
511 MOI of 400. At 1 hour of infection, cells were washed with HBSS 10 times, and media
512 was replaced with DMEM supplemented with 10% FBS, 25 µg/mL gentamicin, and 100
513 mM IPTG. A time-lapsed Z-stack of images was collected with a Nikon Eclipse Ti-2
514 inverted light microscope at 37°C and 5% CO_2 at 10-second intervals for 10 minutes.
515 Images were deconvolved using a Richardson-Lucy algorithm with 20 iterations and all
516 slices within a stack were collapsed into a single image based upon the maximum
517 intensity of pixels in each slice using NIS elements software. For time-lapsed series, in
518 which some focal drift occurred in the XY position, FIJI plugin: Linear Stack Alignment
519 with SIFT, was used to realign timepoints. NIS elements particle tracking software was
520 used to track in-frame bacteria throughout the video to calculate protrusion velocities.
521 Speed was determined for each bacterium by measuring the distance traveled over the
522 duration of time bacterium was in focus.

523 **Live-cell Imaging Analysis for Protrusions Duration:**

524 HeLa cells expressing a membrane-anchored yellow fluorescent protein were seeded at
525 2 X 10^5 cells per well on Ibidi 8-well chamber slides (Ibidi, 80826). The next day, media

526 was replaced with DMEM and 10% FBS and cells were infected with designated strains
527 of *S. flexneri* expressing mCherry at an MOI of 200. At 1 hour of infection, cells were
528 washed with HBSS 10 times, and media was replaced with DMEM supplemented with
529 10% FBS. A time-lapsed Z-stack of images was taken with a Nikon Eclipse Ti-2 inverted
530 light microscope at 37°C and 5% CO_2 at 5-minute intervals for 2.5 hours to examine
531 protrusion duration. Images were deconvolved using a Richardson-Lucy algorithm with
532 20 iterations and all slices within a stack were collapsed into a single image based upon
533 the maximum intensity of pixels in each slice using NIS elements software. Protrusion
534 duration was measured by quantifying the amount of time the bacteria were in each
535 protrusion stage (50).

536 **Quantification of the length of actin tails formed by *L. monocytogenes***

537 HeLa cells were seeded at 8 X 10^5 cells per well in a 6-well plate and cultured for 24
538 hours. The next day, cells were infected with *L. monocytogenes* harboring pGFP (51) at
539 an MOI of 1,500. Bacteria were centrifuged onto cells at 800 *g* for 10 minutes and
540 incubated at 37°C in 5% CO_2. At 90 minutes of infection, cells were washed three times
541 with HBSS, and media was replaced with DMEM with 10% FBS and 25 µg/mL gentamicin.
542 After an additional 3.5 hours, cells were fixed with 3.7% paraformaldehyde for at least 20
543 minutes at room temperature. The cells were permeabilized with 1% triton X-100 in PBS
544 for 30 minutes at room temperature. The cells were washed 5 times with PBS. Cells were
545 stained with phalloidin conjugated to Alexa Flour 750 (Invitrogen A30105), washed with
546 PBS, stained with Hoechst 33342 (Biotech No. 5117), washed twice with PBS, and
547 mounted with Prolong Diamond Antifade Mountant (ThermoFisher, P36930).

548 **Microscopy:**

549 Fluorescent images were acquired on a Nikon Eclipse Ti-2 inverted light microscope
550 equipped with an Orca Fusion BT cMOS camera (Hammamatsu), an IRIS 15 cMOS
551 camera (Photometrics), Semrock Brightline filters, and an Oco stage top incubator
552 chamber that enables regulation of temperature, CO_2, and humidity. NIS elements
553 software (Nikon) was used for image acquisition and analysis. Images were deconvolved
554 using a Richardson-Lucy algorithm with 20 iterations. Microscopic images were pseudo-
555 colored and assembled using Adobe photoshop or FIJI (NIH). Images were collected
556 randomly across the coverslip using an automated imaging pipeline created in NIS
557 elements or the samples were blinded prior to imaging. A minimum of five Z-stacks were
558 collected per coverslip with 0.25 µm step size. To display representative images, all slices
559 within a stack were collapsed into a single image based upon the maximum intensity of
560 pixels in each slice using NIS elements software.

561 **Intensity Analysis:**

562 The signal intensity of random spots of synaptopodin, actin, mDia, Arp2, N-WASP, α-
563 actinin-4 and myosin IIb around bacteria was measured using NIS elements. Three spots
564 were analyzed at each bacterium, and 5-30 bacteria were measured per condition per
565 experiment, and the average intensity was recorded per experiment.

566 **Statistical Analysis:**

567 Statistical difference between means was analyzed with Graph Pad Prism 9. Statistical
568 difference of two means was determined either by Student's t-test or a paired t-test.

569 Unless indicated otherwise, the differences between the means of multiple groups were
570 determined either by two-way ANOVA with Sidak *post hoc* test or by one-way ANOVA
571 with either a Holm-Sidak's *post hoc* test or a Dunnett's *post hoc* test.
572

573 **Acknowledgements**

574 We would like to thank Marcia Goldberg, Vivian Tang, Cammie Lesser, and Hervé
575 Agaisse for reagents. We would like to thank Marcia Goldberg and Marijke Keestra-
576 Gounder and the Keestra-Gounder lab for helpful discussions. We would like to thank
577 Tinalyn Kupfer and the CU | AMC ImmunoMicro Flow Cytometry Shared Resource,
578 RRID:SCR_021321, for assistance with cell sorting. This work was funded by K22
579 AI137296, the GI and Liver Innate Immune Program at the University of Colorado, and
580 the University of Colorado start-up funds to BCR. JER was funded by T32 AI052066.

581 **Author Contributions**

582 J.M.V and B.C.R wrote the initial draft of the manuscript. J.M.V, S.P.C., L.L.L., and B.C.R
583 designed experiments. J.M.V, J.D.T, B.C.R, and J.E.R preformed experiments. All
584 authors discussed the results and commented on the manuscript.

585

COMPETING FINANCIAL INTEREST

The authors declare no competing financial interest.

589 **REFERENCES**

590 1. Dhanda AS, Guttman JA. Localization of host endocytic and actin-associated
591 proteins during *Shigella flexneri* intracellular motility and intercellular spreading. Anat
592 Rec (Hoboken). 2022.
593 2. Stevens JM, Galyov EE, Stevens MP. Actin-dependent movement of bacterial
594 pathogens. Nat Rev Microbiol. 2006;4(2):91-101.
595 3. Hiller G, Weber K, Schneider L, Parajsz C, Jungwirth C. Interaction of assembled
596 progeny pox viruses with the cellular cytoskeleton. Virology. 1979;98(1):142-53.
597 4. Lamason RL, Welch MD. Actin-based motility and cell-to-cell spread of bacterial
598 pathogens. Curr Opin Microbiol. 2017;35:48-57.
599 5. Weddle E, Agaisse H. Principles of intracellular bacterial pathogen spread from
600 cell to cell. PLoS Pathog. 2018;14(12):e1007380.
601 6. Agaisse H. Molecular and Cellular Mechanisms of *Shigella flexneri*
602 Dissemination. Front Cell Infect Microbiol. 2016;6:29.
603 7. Mundel P, Heid HW, Mundel TM, Kruger M, Reiser J, Kriz W. Synaptopodin: an
604 actin-associated protein in telencephalic dendrites and renal podocytes. J Cell Biol.
605 1997;139(1):193-204.
606 8. Chalovich JM, Schroeter MM. Synaptopodin family of natively unfolded, actin
607 binding proteins: physical properties and potential biological functions. Biophys Rev.
608 2010;2(4):181-9.
609 9. Weins A, Schwarz K, Faul C, Barisoni L, Linke WA, Mundel P. Differentiation-
610 and stress-dependent nuclear cytoplasmic redistribution of myopodin, a novel actin-
611 bundling protein. J Cell Biol. 2001;155(3):393-404.

612 10. Asanuma K, Yanagida-Asanuma E, Faul C, Tomino Y, Kim K, Mundel P.
613 Synaptopodin orchestrates actin organization and cell motility via regulation of RhoA
614 signalling. Nat Cell Biol. 2006;8(5):485-91.
615 11. Wang RX, Lee JS, Campbell EL, Colgan SP. Microbiota-derived butyrate
616 dynamically regulates intestinal homeostasis through regulation of actin-associated
617 protein synaptopodin. Proc Natl Acad Sci U S A. 2020;117(21):11648-57.
618 12. Morris T, Sue E, Geniesse C, Brieher WM, Tang VW. Synaptopodin stress fiber
619 and contractomere at the epithelial junction. J Cell Biol. 2022;221(5).
620 13. Hale TL. Genetic basis of virulence in *Shigella* species. Microbiol Rev.
621 1991;55(2):206-24.
622 14. Labrec EH, Schneider H, Magnani TJ, Formal SB. Epithelial Cell Penetration as
623 an Essential Step in the Pathogenesis of Bacillary Dysentery. Journal of bacteriology.
624 1964;88(5):1503-18.
625 15. Goldberg MB, Barzu O, Parsot C, Sansonetti PJ. Unipolar localization and
626 ATPase activity of IcsA, a *Shigella flexneri* protein involved in intracellular movement.
627 Infect Agents Dis. 1993;2(4):210-1.
628 16. Egile C, Loisel TP, Laurent V, Li R, Pantaloni D, Sansonetti PJ, et al. Activation
629 of the CDC42 effector N-WASP by the *Shigella flexneri* IcsA protein promotes actin
630 nucleation by Arp2/3 complex and bacterial actin-based motility. J Cell Biol.
631 1999;146(6):1319-32.
632 17. Bernardini ML, Mounier J, d'Hauteville H, Coquis-Rondon M, Sansonetti PJ.
633 Identification of icsA, a plasmid locus of *Shigella flexner*i that governs bacterial intra-

634 and intercellular spread through interaction with F-actin. Proceedings of the National
635 Academy of Sciences of the United States of America. 1989;86(10):3867-71.
636 18. Kadurugamuwa JL, Rohde M, Wehland J, Timmis KN. Intercellular spread of
637 *Shigella flexneri* through a monolayer mediated by membranous protrusions and
638 associated with reorganization of the cytoskeletal protein vinculin. Infect Immun.
639 1991;59(10):3463-71.
640 19. Campbell-Valois FX, Sachse M, Sansonetti PJ, Parsot C. Escape of Actively
641 Secreting *Shigella flexneri* from ATG8/LC3-Positive Vacuoles Formed during Cell-To-
642 Cell Spread Is Facilitated by IcsB and VirA. mBio. 2015;6(3):e02567-14.
643 20. Sansonetti PJ, Arondel J, Fontaine A, d'Hauteville H, Bernardini ML. OmpB
644 (osmo-regulation) and icsA (cell-to-cell spread) mutants of *Shigella flexneri*: vaccine
645 candidates and probes to study the pathogenesis of shigellosis. Vaccine.
646 1991;9(6):416-22.
647 21. Suzuki T, Sasakawa C. Molecular basis of the intracellular spreading of *Shigella.*
648 Infect Immun. 2001;69(10):5959-66.
649 22. Yum LK, Byndloss MX, Feldman SH, Agaisse H. Critical role of bacterial
650 dissemination in an infant rabbit model of bacillary dysentery. Nat Commun.
651 2019;10(1):1826.
652 23. Mitchell PS, Roncaioli JL, Turcotte EA, Goers L, Chavez RA, Lee AY, et al.
653 NAIP-NLRC4-deficient mice are susceptible to shigellosis. Elife. 2020;9.
654 24. Robbins JR, Barth AI, Marquis H, de Hostos EL, Nelson WJ, Theriot JA. *Listeria*
655 *monocytogenes* exploits normal host cell processes to spread from cell to cell. J Cell
656 Biol. 1999;146(6):1333-50.

657 25. Ichimura K, Kurihara H, Sakai T. Actin filament organization of foot processes in
658 rat podocytes. J Histochem Cytochem. 2003;51(12):1589-600.
659 26. Yap K, Drakew A, Smilovic D, Rietsche M, Paul MH, Vuksic M, et al. The actin-
660 modulating protein synaptopodin mediates long-term survival of dendritic spines. Elife.
661 2020;9.
662 27. Heindl JE, Saran I, Yi CR, Lesser CF, Goldberg MB. Requirement for formin-
663 induced actin polymerization during spread of *Shigella flexneri*. Infection and immunity.
664 2010;78(1):193-203.
665 28. Fattouh R, Kwon H, Czuczman MA, Copeland JW, Pelletier L, Quinlan ME, et al.
666 The diaphanous-related formins promote protrusion formation and cell-to-cell spread of
667 *Listeria monocytogene*s. J Infect Dis. 2015;211(7):1185-95.
668 29. Bishai EA, Sidhu GS, Li W, Dhillon J, Bohil AB, Cheney RE, et al. Myosin-X
669 facilitates *Shigella*-induced membrane protrusions and cell-to-cell spread. Cellular
670 microbiology. 2013;15(3):353-67.
671 30. Dragoi AM, Agaisse H. The serine/threonine kinase STK11 promotes *Shigella*
672 *flexneri* dissemination through establishment of cell-cell contacts competent for tyrosine
673 kinase signaling. Infect Immun. 2014;82(11):4447-57.
674 31. Monack DM, Theriot JA. Actin-based motility is sufficient for bacterial membrane
675 protrusion formation and host cell uptake. Cell Microbiol. 2001;3(9):633-47.
676 32. Theriot JA, Mitchison TJ, Tilney LG, Portnoy DA. The rate of actin-based motility
677 of intracellular *Listeria monocytogenes* equals the rate of actin polymerization. Nature.
678 1992;357(6375):257-60.

679 33. Gerbal F, Chaikin P, Rabin Y, Prost J. An elastic analysis of *Listeria*
680 *monocytogenes* propulsion. Biophys J. 2000;79(5):2259-75.
681 34. Giardini PA, Fletcher DA, Theriot JA. Compression forces generated by actin
682 comet tails on lipid vesicles. Proc Natl Acad Sci U S A. 2003;100(11):6493-8.
683 35. Buvall L, Rashmi P, Lopez-Rivera E, Andreeva S, Weins A, Wallentin H, et al.
684 Proteasomal degradation of Nck1 but not Nck2 regulates RhoA activation and actin
685 dynamics. Nat Commun. 2013;4:2863.
686 36. Moreau V, Frischknecht F, Reckmann I, Vincentelli R, Rabut G, Stewart D, et al.
687 A complex of N-WASP and WIP integrates signalling cascades that lead to actin
688 polymerization. Nat Cell Biol. 2000;2(7):441-8.
689 37. Schuch R, Sandlin RC, Maurelli AT. A system for identifying post-invasion
690 functions of invasion genes: requirements for the Mxi-Spa type III secretion pathway of
691 *Shigella flexneri* in intercellular dissemination. Mol Microbiol. 1999;34(4):675-89.
692 38. Duncan-Lowey JK, Wiscovitch AL, Wood TE, Goldberg MB, Russo BC. *Shigella*
693 *flexneri* Disruption of Cellular Tension Promotes Intercellular Spread. Cell Rep.
694 2020;33(8):108409.
695 39. Kuehl CJ, Dragoi AM, Agaisse H. The *Shigella flexneri* type 3 secretion system is
696 required for tyrosine kinase-dependent protrusion resolution, and vacuole escape during
697 bacterial dissemination. PLoS One. 2014;9(11):e112738.
698 40. Nasser A, Mosadegh M, Azimi T, Shariati A. Molecular mechanisms of *Shigella*
699 effector proteins: a common pathogen among diarrheic pediatric population. Mol Cell
700 Pediatr. 2022;9(1):12.

701 41. Ernst NH, Reeves AZ, Ramseyer JE, Lesser CF. High-Throughput Screening of
702 Type III Secretion Determinants Reveals a Major Chaperone-Independent Pathway.
703 mBio. 2018;9(3).
704 42. Gall TL, Mavris M, Martino MC, Bernardini ML, Denamur E, Parsot C. Analysis of
705 virulence plasmid gene expression defines three classes of effectors in the type III
706 secretion system of *Shigella flexneri*. Microbiology (Reading). 2005;151(Pt 3):951-62.
707 43. Kane CD, Schuch R, Day WA, Jr., Maurelli AT. MxiE regulates intracellular
708 expression of factors secreted by the *Shigella flexneri* 2a type III secretion system. J
709 Bacteriol. 2002;184(16):4409-19.
710 44. Hall CP, Jadeja NB, Sebeck N, Agaisse H. Characterization of MxiE- and H-NS-
711 Dependent Expression of ipaH7.8, ospC1, yccE, and yfdF in *Shigella flexneri*. mSphere.
712 2022;7(6):e0048522.
713 45. Vlachos A, Korkotian E, Schonfeld E, Copanaki E, Deller T, Segal M.
714 Synaptopodin regulates plasticity of dendritic spines in hippocampal neurons. J
715 Neurosci. 2009;29(4):1017-33.
716 46. Lum M, Morona R. Myosin IIA is essential for *Shigella flexneri* cell-to-cell spread.
717 Pathog Dis. 2014;72(3):174-87.
718 47. Moore AS, Coscia SM, Simpson CL, Ortega FE, Wait EC, Heddleston JM, et al.
719 Actin cables and comet tails organize mitochondrial networks in mitosis. Nature.
720 2021;591(7851):659-64.
721 48. Erard M, Fredj A, Pasquier H, Beltolngar DB, Bousmah Y, Derrien V, et al.
722 Minimum set of mutations needed to optimize cyan fluorescent proteins for live cell
723 imaging. Mol Biosyst. 2013;9(2):258-67.

724 49. Eshleman EM, Bortell N, McDermott DS, Crisler WJ, Lenz LL. Myeloid cell
725 responsiveness to interferon-gamma is sufficient for initial resistance to *Listeria*
726 *monocytogenes*. Curr Res Immunol. 2020;1:1-9.
727 50. Weddle EA, Koseoglu VK, DeVasure BA, Agaisse HF. The type three secretion
728 system effector protein IpgB1 promotes *Shigella flexneri* cell-to-cell spread through
729 double-membrane vacuole escape. PLoS Pathog. 2022;18(2):e1010380.
730 51. Cole C, Thomas S, Filak H, Henson PM, Lenz LL. Nitric oxide increases
731 susceptibility of Toll-like receptor-activated macrophages to spreading *Listeria*
732 *monocytogenes*. Immunity. 2012;36(5):807-20.
733

734 **FIGURE LEGENDS**

735 **Figure 1: Synaptopodin is required for efficient intercellular spread of *S. flexneri***

736 Monolayers of T84 (A-B), MDCK (C-D), or HeLa (E-F) cells that produce a control or
737 synaptopodin specific shRNA were infected with *S. flexneri* and stained with neutral red
738 at 48 hours of infection. (A, C, and E) Representative images. Dotted lines indicate plaque
739 boundary. Scale bar, 0.5 mm. (B, D, and F) Quantification of the area of plaques from
740 images represented in A, C, and E. 15-60 plaques measured per condition per
741 experiment. Dots are independent experiments. *, $p<0.05$ by paired t-test (B and D) or by
742 one-way ANOVA with Dunnett's *post hoc* test (F). Data are mean ± SEM.

743 **Figure 2: Synaptopodin is required for protrusion formation by *S. flexneri***

744 (A) Representative images of HeLa cells infected with *S. flexneri.* Cyan, *S. flexneri;*
745 magenta, actin; blue, DNA. Arrows, bacteria in protrusions. Scale bar, 5 μM. 5-10 fields
746 were analyzed per condition per experiment. (B) Quantification of the percentage of
747 intracellular bacteria within a protrusion. (C) Quantification of the intensity of actin in
748 protrusions. (B and C) Dots are independent experiments. (D) Quantification of the length
749 of protrusions. Tukey method used to define whiskers. (B-D) N.S., not significant; *,
750 $p<0.05$ by one-way ANOVA with Holm-Sidak's *post hoc* test. (E-G) Time lapse images
751 videos of bacteria forming plasma membrane protrusions. (E) Representative images of
752 protrusion formation. Cyan, S. *flexneri;* green, plasma membrane. Scale bar 5 μM.
753 Arrows, bacteria in protrusions; dot, protrusion origination point; dotted line, progression
754 of protrusion formation. (F) Quantification of the speed of protrusion formation from videos
755 represented in E. (G) Quantification of the duration bacteria remain in protrusions. (F-G)

756 Dots are individual bacteria, pooled from 3 independent experiments. *, p<0.05 by
757 Student's t-test. Data are mean ± SEM.

758 **Figure 3: Synaptopodin regulates actin tail formation by *S. flexneri***

759 Infection of HeLa cells infected with *S. flexneri* for 90 min. (A) Representative images.
760 Cyan, *S. flexneri;* magenta, actin; blue, DNA. Arrows, bacteria with actin tails. Dotted line,
761 trace of actin tail. Scale bar, 5 μM. (B) Quantification of percentage of bacteria with actin
762 tails. (C) Quantification of the length of actin tails. (D-E) Time-lapsed microscopy of HeLa
763 cells producing a membrane anchored YFP infected with *S. flexneri* producing CFP. (D)
764 Representative still images from time-lapsed videos for 2 minutes from initial observation
765 of motility. Cyan, *S. flexneri*; green, plasma membrane. Dots are the position of bacteria
766 at each time point, dotted line is arbitrary straight line between dots showing bacterial
767 progression over time. Scale bar, 5 μM. (E) Quantification of the speed at which bacteria
768 move in the cytosol from videos represented in E. Mean indicated by bar. (B, C) 5-10
769 fields were analyzed per experiment. Dots are independent experiments. Data are mean
770 ± SEM. N.S., not significant; *, p<0.05; **, p<0.1; ***, p<0.001 by one-way ANOVA with
771 Dunnett's *post hoc* test. (E) N.S., not significant; *, p<0.05 by Student's t-test. Dots are
772 individual bacteria pooled together from three experiments. (F) Schematic depicting
773 shorter tails are formed in cells lacking synaptopodin compared to tails formed in control
774 cells. Generated with BioRender.

775 **Figure 4: Synaptopodin is required for Myosin IIb recruitment around bacteria**

776 HeLa cells were infected with *S. flexneri* for 90 min. (A) Representative images. Cyan, *S.*
777 *flexneri*; magenta, actin; red, myosin IIb; blue, DNA. Arrows, bacteria with myosin IIb.

778 Scale bar, 5 μM. (B) Quantification of percentage of bacteria with myosin IIb. (C)
779 Quantification of the intensity of myosin IIb around bacteria. (D) Representative images
780 depicting α-actinin-4 recruitment around bacteria. Cyan, *S. flexneri;* magenta, actin; red,
781 α-actinin-4; blue, DNA. Arrows, bacteria with α-actinin-4. Scale bar, 5 μM. (E)
782 Quantification of the percentage of bacteria with α-actinin-4. (F) Quantification of the
783 intensity of α-actinin-4. (B-C and E-F) 5-10 fields were analyzed per condition per
784 experiment. Dots are independent experiments. Data are mean ± SEM. NS, not
785 significant; *, $p<0.05$; **, $p<0.01$ by one-way ANOVA with Dunnett's *post hoc* test.

786 **Figure 5: Synaptopodin is recruited around *S. flexneri* in an IcsA and a type 3**
787 **secretion system dependent manner**

788 Control HeLa cells were infected for 90 min with *S. flexneri* strains. (A) Representative
789 images. Cyan, *S. flexneri*; magenta, actin; red, synaptopodin (synpo); blue, DNA. Arrows,
790 bacteria with actin and synaptopodin. Scale bar, 5 μM. (B) Quantification of the
791 percentage of bacteria with actin. (C) Quantification of the percentage of bacteria with
792 synaptopodin. (D) Quantification of the intensity of actin around bacteria. (E)
793 Quantification of intensity of synaptopodin around bacteria. (B-E) 5-10 fields were
794 analyzed per condition per experiment. Dots are independent experiments. Data are
795 mean ± SEM. N.D., not detected. NS, not significant; *, $p<0.05$; **, $p<0.01$ by one-way
796 ANOVA with Dunnett's *post hoc* test.

797 **Fig. 6. Schematic of *S. flexneri* intercellular spread in control versus**

798 **synaptopodin knockdown cell lines.**

799 Schematic of *S. flexneri* intercellular lifecycle. (I) *S. flexneri* induces its uptake into cells.
800 (II) Following uptake, it is present in a vacuole. (III) It escapes the vacuole into the cytosol
801 where the bacteria replicate. A portion of the bacteria nucleate the polymerization of actin,
802 which enables the bacteria to move in the cell cytosol. (V) Bacteria near the cell periphery
803 deform the plasma membrane into a protrusion. (VI) The protrusion resolves into a double
804 membrane vacuole. (VII) The bacteria escape the double membrane vacuole into the
805 cytosol. (A) Cells with synaptopodin enabled bacteria to form actin tails that are longer
806 and more aligned with the bacteria than cells lacking synaptopodin. Bacteria in cells with
807 synaptopodin form protrusions at a higher velocity that resolve more quickly (V). (B) In
808 cells lacking synaptopodin, the actin tails are shorter. Protrusions are formed at a slower
809 velocity and take longer to resolve into a double membrane vacuole (V). (A-B) 1. Bacteria
810 lacking IcsA do not polymerize actin or recruit synaptopodin. 2. Polar localization of IcsA
811 is associated with synaptopodin recruitment, and IcsA recruits N-WASP and Apr2/3
812 irrespective of synaptopodin abundance in cells. 3. Synaptopodin recruitment to bacteria
813 is further enhanced in a type 3 secretion dependent manner. Created with biorender.com

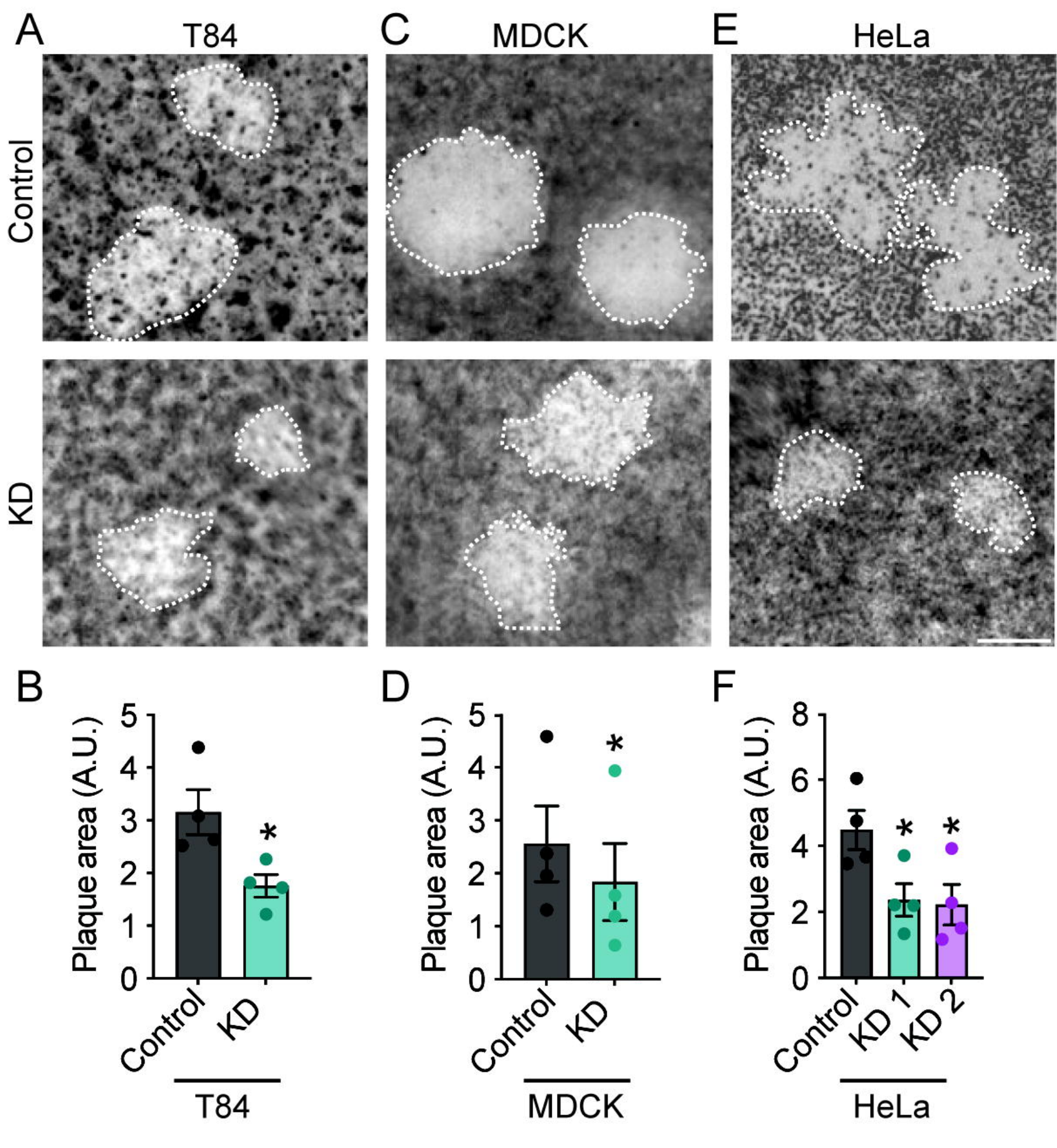
A
T84
C
MDCK
E
HeLa
Control
KD
B
Plaque area (A.U.)
5
4
3
2
1
0
*
Control
KD
T84
D
Plaque area (A.U.)
5
4
3
2
1
0
*
Control
KD
MDCK
F
Plaque area (A.U.)
8
6
4
2
0
*
*
Control
KD 1
KD 2
HeLa

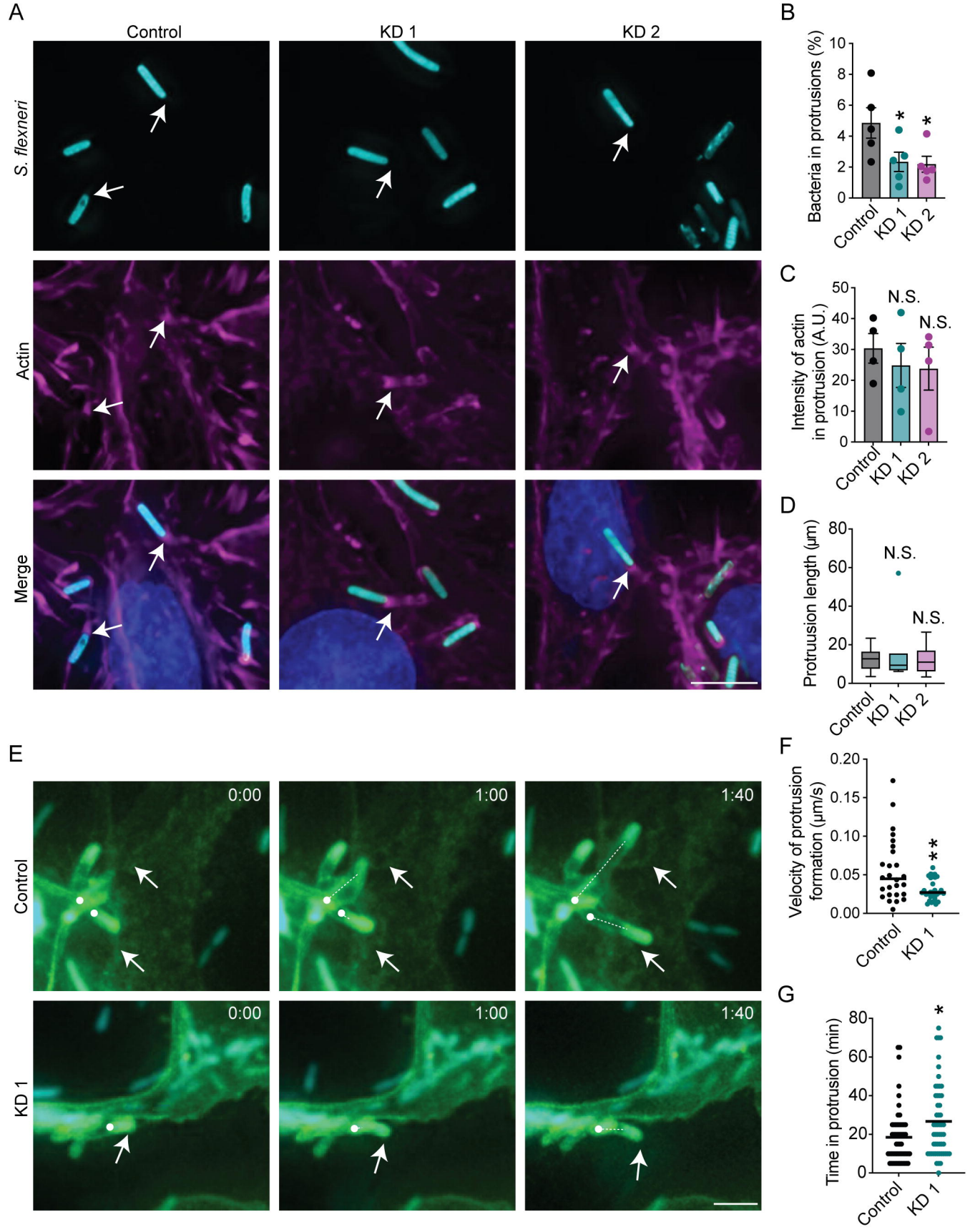
A
Control
KD 1
KD 2
S. flexneri
Actin
Merge
B
Bacteria in protrusions (%)
Control
KD 1
KD 2
C
Intensity of actin in protrusion (A.U.)
N.S.
N.S.
D
Protruusion length (µm)
N.S.
N.S.
E
0:00
1:00
1:40
Control
KD 1
F
Velocity of protrusion formation (µm/s)
G
Time in protrusion (min)

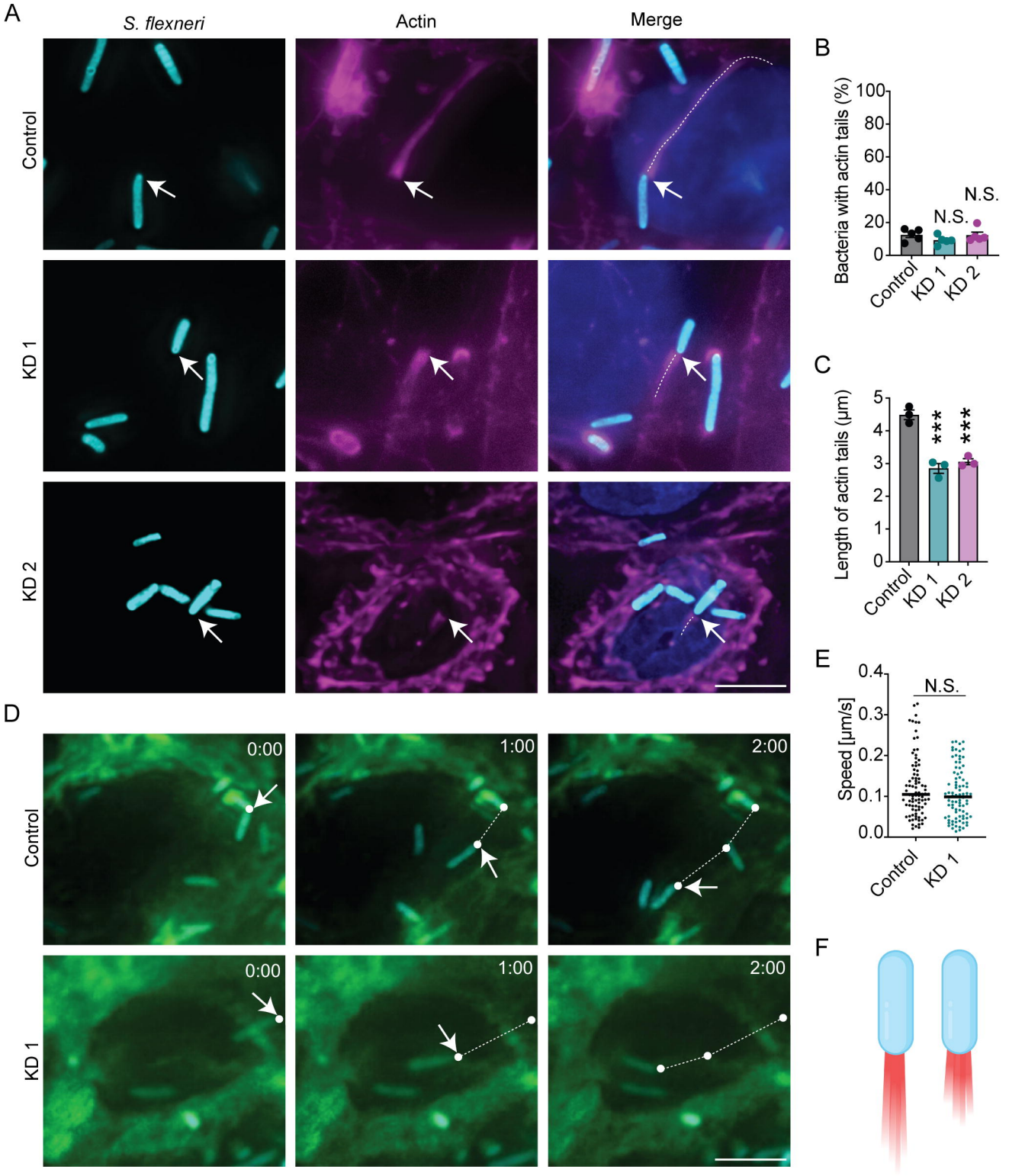
A
S. flexneri
Actin
Merge
Control
KD 1
KD 2
B
Bacteria with actin tails (%)
100
80
60
40
20
0
N.S.
N.S.
Control
KD 1
KD 2
C
Length of actin tails (µm)
5
4
3
2
1
0
***
***
Control
KD 1
KD 2
D
0:00
1:00
2:00
Control
KD 1
E
Speed [µm/s]
0.4
0.3
0.2
0.1
0.0
N.S.
Control
KD 1
F

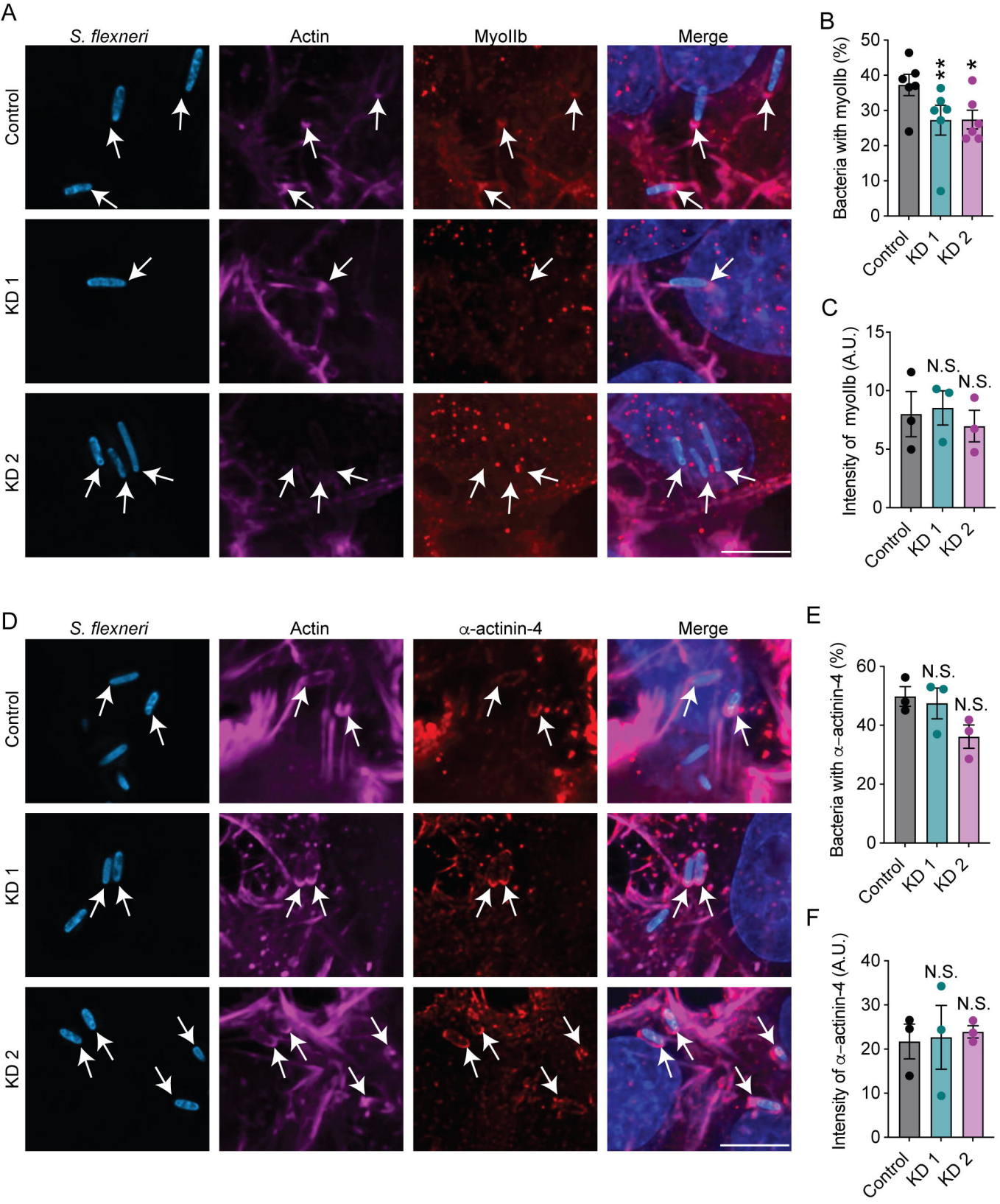
A
S. flexneri
Actin
MyoIIb
Merge
Control
KD 1
KD 2
B
Bacteria with myoIIb (%)
50
40
30
20
10
0
**
*
Control
KD 1
KD 2
C
Intensity of myoIIb (A.U.)
15
10
5
0
N.S.
N.S.
Control
KD 1
KD 2
D
S. flexneri
Actin
α-actinin-4
Merge
Control
KD 1
KD 2
E
Bacteria with α-actinin-4 (%)
60
40
20
0
N.S.
N.S.
Control
KD 1
KD 2
F
Intensity of α-actinin-4 (A.U.)
40
30
20
10
0
N.S.
N.S.
Control
KD 1
KD 2

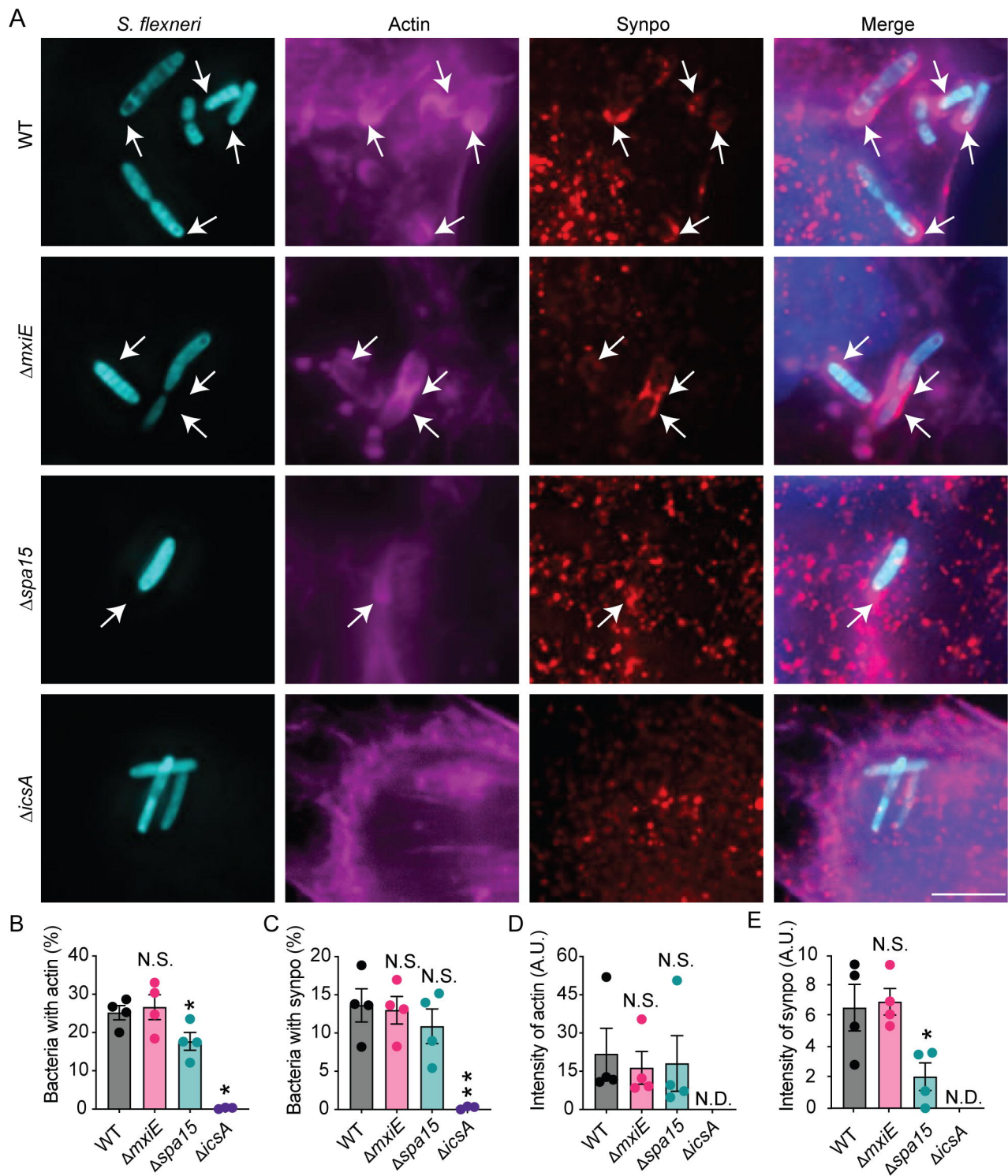
A
S. flexneri
Actin
Synpo
Merge
WT
ΔmxiE
Δspa15
ΔicsA
B
Bacteria with actin (%)
N.S.
*
*
C
Bacteria with synpo (%)
N.S.
N.S.
*
*
D
Intensity of actin (A.U.)
N.S.
N.S.
N.D.
E
Intensity of synpo (A.U.)
N.S.
*
N.D.
WT
ΔmxiE
Δspa15
ΔicsA

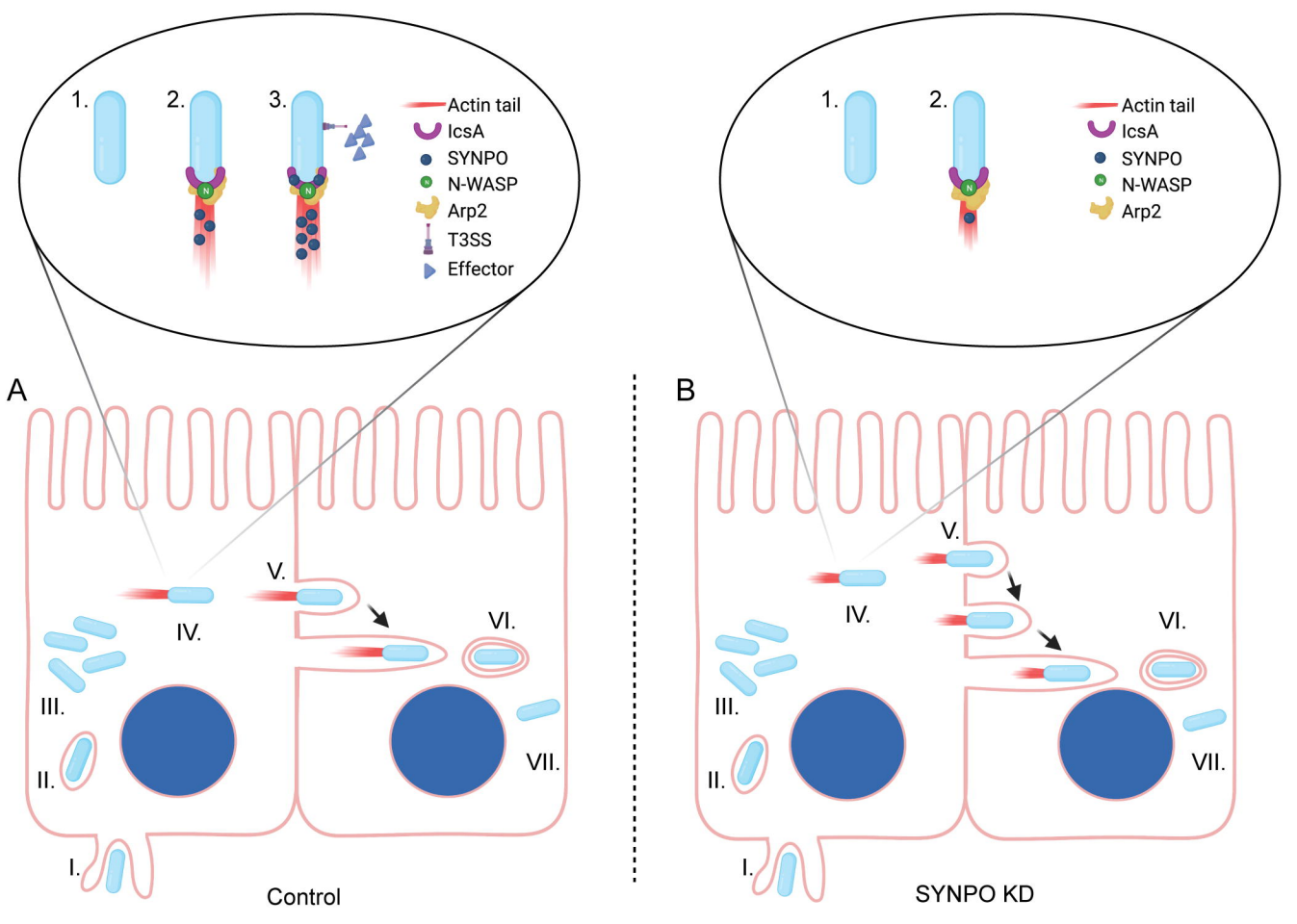
1.
2.
3.
Actin tail
IcsA
SYNPO
N-WASP
Arp2
T3SS
Effector
A
I.
II.
III.
IV.
V.
VI.
VII.
Control
B
1.
2.
Actin tail
IcsA
SYNPO
N-WASP
Arp2
I.
II.
III.
IV.
V.
VI.
VII.
SYNPO KD